ELSEVIER

Turbulent heat and mass transfer in an asymmetrically heated, vertical parallel-plate channel

A. G. Fedorov, R. Viskanta and A. A. Mohamad*
Heat Transfer Laboratory, School of Mechanical Engineering, Purdue University, West Lafayette, IN

An analysis has been developed to predict combined heat and mass transfer from an evaporating water film falling under gravity along a heated vertical plate with countercurrent air flow in the parallel-plate channel. The problem considered is related to numerous industrial processing operations and to containment cooling of advanced nuclear reactors. A low-Reynolds number k-ε turbulence model is used in conjunction with combined heat and mass transfer analysis in an asymmetrically heated, parallel-plate vertical channel. The heated wall is wetted with a film of water that flows down by the force of gravity, and countercurrently flowing air cools the water film. The model predictions are first compared with available experimental data for the purpose of validating the model. The local heat fluxes, Nusselt, and Sherwood numbers are reported to obtain understanding of the physical phenomena.

Keywords: heat and mass transfer; turbulent natural convection; evaporating film

Introduction

Heat transfer augmentation through cooling associated with liquid evaporation in turbulent convection is important in many engineering applications. Notable examples include cooling towers, waste heat disposal in process industry, protection of system components from a high-temperature gas stream, and many others. The purpose of this article is to report on a study of evaporative cooling by analyzing combined heat and mass transfer processes to a turbulent gas stream in countercurrent flow from a thin liquid film falling along a vertical wall of a parallel-plate channel.

Analysis of combined heat and mass transfer to/from an evaporating liquid film has been reported (Yan et al. 1989; Tsay and Lin 1990). A large, adiabatic, vertical plate was wetted by a water film, and a laminar gas stream was in parallel, cocurrent, boundary-layer flow. Mixed-convection heat and mass transfer in a wetted vertical channel has also been analyzed (Yan 1991; Yan 1995a). Very recently, Ambrosini et al. (1995) have reported on an experimental study of combined heat and mass transfer in an asymmetrically heated vertical, parallel-plate channel. Reference is made to recent publications (Tsay and Lin 1990; Yan 1995a, b; Ambrosini et al. 1995) for a more complete discussion of the earlier studies. A thorough review of the literature has failed to identify any relevant theoretical studies of the problem discussed in this article.

*Present address: Department of Mechanical Engineering, Eastern Mediterranean University, Mersin 10, Turkey.

Address reprint requests to Dr. R. Viskanta, Heat Transfer Laboratory, Purdue University, School of Mechanical Engineering, 1288 School of Mech. Eng. Bldg., West Lafayette, IN 47907-1288, USA.

Received 12 July 1996; accepted 23 September 1996

Int. J. Heat and Fluid Flow 18: 307–315, 1997

655 Avenue of the Americas, New York, NY 10010

0142-727X/97/$17.00
PII S0142-727X(97)00010-6

Analysis

Physical model and assumptions

Consider an asymmetrically heated vertical, parallel-plate channel shown schematically in Figure 1. The left wall of the channel is wet and is heated by imposing a uniform wall temperature. The right wall of the channel (slot) is dry and adiabatic. The air–water mixture enters the channel at temperature T_o. For the sake of generality, we consider the case where the velocity of a moist air entering the channel may be sufficiently small so that the buoyancy force may be sufficiently large in comparison with the pressure force and must be retained in the y-momentum equation. The transport processes are considered steady and the flow incompressible. The following additional assumptions are made in the analysis.

(1) The thermodynamic and thermophysical properties of air, water, and air–water vapor mixture are functions of both local temperature and composition. The variation of the thermophysical properties with temperature and concentration is accounted for using published information (Tsay and Lin 1990).

(2) Thermal diffusion (Soret), diffusion-thermo (Dufour), and interdiffusion effects are neglected in comparison to advection.

(3) Viscous heat dissipation and thermal radiation are neglected in comparison to advection.

(4) The left heated wall is considered to be fully covered by a thin water film. The film is assumed to be very thin, of uniform thickness, and not to be affected or to interact with the air stream.

(5) Thermodynamic equilibrium is assumed at the water film–air interface when computing the mass fraction of the water vapor.

Model equations

The time-averaged Navier–Stokes equations of motion for steady, two-dimensional (2-D) incompressible flow in a vertical channel can be written as follows.

Conservation of mass (continuity):

$$\frac{\partial(\rho u)}{\partial x}+\frac{\partial(\rho v)}{\partial y}=0 \tag{1}$$

Conservation of x-momentum:

$$\frac{\partial}{\partial x}(\rho uu)+\frac{\partial}{\partial y}(\rho uv)=-\frac{\partial p}{\partial x}+\frac{\partial}{\partial x}\left[(\mu+\mu_t)\frac{\partial u}{\partial x}\right]+\frac{\partial}{\partial y}\left[(\mu+\mu_t)\frac{\partial u}{\partial y}\right]-\frac{2}{3}\rho\frac{\partial k}{\partial x} \tag{2}$$

Conservation of y-momentum:

$$\frac{\partial}{\partial x}(\rho uv)+\frac{\partial}{\partial y}(\rho vv)=-\frac{\partial p}{\partial y}+\frac{\partial}{\partial x}\left[(\mu+\mu_t)\frac{\partial v}{\partial x}\right]+\frac{\partial}{\partial y}\left[(\mu+\mu_t)\frac{\partial v}{\partial y}\right]-\frac{2}{3}\rho\frac{\partial k}{\partial y}+(\rho-\rho_o)g \tag{3}$$

Conservation of energy equation:

$$\frac{\partial}{\partial x}(\rho uT)+\frac{\partial}{\partial y}(\rho vT)=\frac{\partial}{\partial x}\left[\left(\frac{k}{c_p}+\frac{\mu_t}{\mathrm{Pr}_t}\right)\frac{\partial T}{\partial x}\right]+\frac{\partial}{\partial y}\left[\left(\frac{k}{c_p}+\frac{\mu_t}{\mathrm{Pr}_t}\right)\frac{\partial T}{\partial y}\right] \tag{4}$$

Conservation of species (water vapor):

$$\frac{\partial}{\partial x}(\rho u\omega)+\frac{\partial}{\partial y}(\rho v\omega)=\frac{\partial}{\partial x}\left[\rho\left(D+\frac{\nu_t}{\mathrm{Sc}_t}\right)\frac{\partial \omega}{\partial x}\right]+\frac{\partial}{\partial y}\left[\rho\left(D+\frac{\nu_t}{\mathrm{Sc}_t}\right)\frac{\partial \omega}{\partial y}\right] \tag{5}$$

The superscript bar (−) usually employed to denote time-averaged dependent variables is neglected for the sake of simplicity in notation. In Equations 2–5, μ_t is the turbulent dynamic viscosity that is to be predicted from the knowledge of the kinetic energy of turbulence k and turbulent kinetic energy dissipation rate ε. Note that in the above formulation, the variations of the thermophysical properties with temperature and air–water vapor composition are included.

Notation

C_1, C_2, C_3, C_μ	empirical constants in the k-ε turbulence model
c_p	specific heat (J/kg K)
D	diffusion coefficient (m^2/s)
f_1, f_2, f_μ	functions in the k-ε turbulence model
G	generation term in turbulence equations, Equation 8
g	mass transfer coefficient, $-D\cdot\partial\omega/\partial x\|_w/(\omega_w-\omega_b)$ (m/s)
H	height of parallel-plate channel, Figure 1, m
h	heat transfer coefficient, $-k\cdot\partial T/\partial x\|_w/(T_w-T_b)$ (W/m^2K)
h_{fg}	latent heat of evaporation (J/kg)
k	kinetic energy of turbulence (m^2/s^2) or thermal conductivity (W/m K)
M	molecular weight (kg/mol)
m	evaporative mass flux (kg/m^2s)
Nu	Nusselt number, Equation 20
Pr	Prandtl number, $\mu c_p/k$ or ν/α
Pr_t	turbulent Prandtl number, $\mu_t c_p/k_t$
p	pressure (Pa)
Re	Reynolds number, $\rho v_o D_h/\mu$
Re_t	turbulent Reynolds number, $k^2/\varepsilon\nu$
Sc	Schmidt number, ν/D
Sc_t	turbulent Schmidt number, ν_t/D_t
Sh	Sherwood number, Equation 21
T	temperature, (K)
u	horizontal velocity component in the x-direction (m/s)
v	vertical velocity component in the y-direction (m/s)
W	channel width, Figure 1, m
x	coordinate as defined in Figure 1, m
y	coordinate as defined in Figure 1, m

Greek

α	thermal diffusivity, $k/\rho c_p$ (m^2/s)
δ	thickness of water film, (m)
ε	dissipation rate of turbulent kinetic energy (m^2/s^3)
μ	dynamic viscosity (Pa·s)
ν	kinematic viscosity (m^2/s)
ρ	density (kg/m^3)
$\sigma_k, \sigma_\varepsilon$	turbulent Prandtl and Schmidt numbers for k and ε
ω	mass fraction

Subscripts

a	air
b	bulk gas
c	cold wall
H	height of channel (see Figure 1)
h	hot wall
i	water film–air interface
k	kinetic energy
l	latent
s	sensible
t	turbulent quantity
v	water vapor
y	local quantity in the y-direction
ε	turbulent kinetic energy dissipation
o	inlet of channel

Superscript

−	averaged quantities

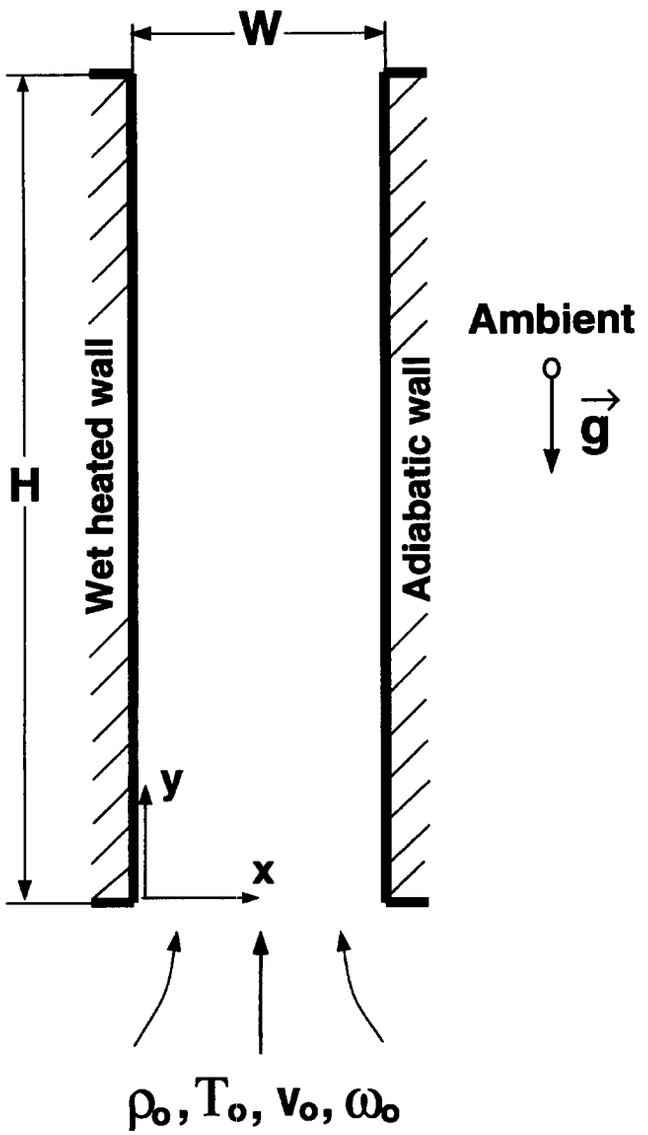

Figure 1 Schematic diagram and coordinate system for forced-convection in a vertical, parallel-plate channel

The transport equations for k and ε can be calculated using the low-Reynolds number k-ε turbulence model. These equations can be derived from the Navier–Stokes equations of motion and are given as (To and Humphrey 1987; Yan 1995b).

Turbulence kinetic energy (k-*equation*):

$$\frac{\partial}{\partial x}(\rho u k)+\frac{\partial}{\partial y}(\rho v k)=\frac{\partial}{\partial x}\left[\left(\mu+\frac{\mu_t}{\sigma_k}\right)\frac{\partial k}{\partial x}\right]+\frac{\partial}{\partial y}\left[\left(\mu+\frac{\mu_t}{\sigma_k}\right)\frac{\partial k}{\partial y}\right]-\rho\varepsilon+\frac{g}{\rho}\left(\frac{\mu_t}{\mathrm{Pr}_t}\right)\frac{\partial \rho}{\partial y}+G \tag{6}$$

Dissipation of turbulent kinetic energy (ε-*equation*):

$$\frac{\partial}{\partial x}(\rho u \varepsilon)+\frac{\partial}{\partial y}(\rho v \varepsilon)=\frac{\partial}{\partial x}\left[\left(\mu+\frac{\mu_t}{\sigma_\varepsilon}\right)\frac{\partial \varepsilon}{\partial x}\right]+\frac{\partial}{\partial y}\left[\left(\mu+\frac{\mu_t}{\sigma_\varepsilon}\right)\frac{\partial \varepsilon}{\partial y}\right]+C_1\left(\frac{\varepsilon}{k}\right)G-C_2 f_2 \rho \varepsilon^2/k+C_3\frac{g}{\rho}\left(\frac{\mu_t \varepsilon}{\mathrm{Pr}_t k}\right)\frac{\partial \rho}{\partial y} \tag{7}$$

where

$$G=\mu_t\left(\frac{\partial u_i}{\partial x_j}+\frac{\partial u_j}{\partial x_i}\right)\frac{\partial u_i}{\partial x_j}-\frac{2}{3}k\delta_{ij}\frac{\partial u_i}{\partial x_j} \tag{8}$$

In the conservation equations and the k-ε turbulence model equations, the turbulent dynamic (eddy) viscosity μ_t is related to k and ε by

$$\mu_t=C_\mu \rho f_\mu (k^2/\varepsilon) \tag{9}$$

The appropriate constants, factors, turbulent Prandtl and Schmidt numbers, as well as the low-Reynolds number wall-damping functions f_μ, f_1, and f_2 are not well known for turbulent, buoyancy-driven convective flows, although they have been generated and optimized for forced-convection boundary-layer flows (Jones and Launder 1973; Patel et al. 1985; Launder 1988). For lack of a better choice, these results for forced convection flows are retained in the present analysis for natural convection. The values of constants and functions are listed in Table 1.

Because the flow involves combined heat and mass transfer, turbulent Prandtl and Schmidt numbers must be specified. Calculations with a constant value of $\mathrm{Pr}_t = 0.9$ across the boundary layer show no pronounced effect on the heat transfer coefficient (i.e., Stanton number) and temperature distributions (Patel et al. 1985). Therefore, a value of $\mathrm{Pr}_t = \mathrm{Sc}_t = 0.9$ is used in the calculations.

Boundary conditions

A no-slip boundary condition is imposed on the velocity components at the walls. For mixed-convection, the velocity at the inlet is specified, and the velocity gradient is set to zero at the outlet. The transverse velocity component u of the air–vapor mixture at the wetted wall ($x = 0$) is deduced by assuming the interface to be semipermeable (Eckert and Drake 1972). That is, the solubility of air in liquid water is negligibly small, and the x-direction

Table 1 Constants and functions for the low-Reynolds number k-ε turbulence model

C_1	1.44
C_2	1.8
C_3	1.5
C_μ	0.09
Pr_t	0.9
Sc_t	0.9
σ_k	1.0
σ_ε	1.3
f_1	1.0
f_2	$1.0-0.3\exp(-\mathrm{Re}_t^2)$
f_μ	$\exp[-3.4/(1+\mathrm{Re}_t/50)^2]$

velocity of air is zero at the water film–air interface.

$$u_i = m_i/\rho = -\frac{D}{(1-\omega_i)}\frac{\partial \omega}{\partial x} \qquad \text{at} \qquad x = 0 \tag{10}$$

where ω_i is the mass fraction of water vapor at the water film–air interface ($x = 0$). By assuming that the interface is at thermodynamic equilibrium and the air–water vapor mixture is an ideal gas mixture, the mass fraction of water vapor ω_i can be calculated by

$$\omega_i = \frac{M_v p_{v,i}}{M_a(p - p_{v,i}) + M_v p_{v,i}} \tag{11}$$

where $p_{v,i}$ is the partial pressure of the water vapor evaluated at the interfacial temperature.

The boundary conditions for k and ε at the wall, consistent with the equations for the low-Reynolds number k-ε turbulence model, are (To and Humphrey 1987)

$$k = 0 \quad \textit{at walls} \tag{12}$$

and

$$\varepsilon = 2(\mu/\rho)\left(\frac{\partial k^{1/2}}{\partial x}\right)^2 \quad \textit{at walls}. \tag{13}$$

To initiate the calculation of k- and ε-equations, the initial conditions for k and ε must be specified. The kinetic energy of turbulence at the inlet is given by

$$k = k_o = \frac{3}{2}Tu_o v_o^2 \tag{14}$$

where Tu_o is the turbulence intensity at the inlet to the channel. The initial value of the turbulent kinetic energy dissipation rate ε at inlet is given by

$$\varepsilon_o = (\mu/\rho)\left(\frac{C_\mu}{\kappa}\right)\left(\frac{\rho k^{3/2}}{\mu x_w}\right) \tag{15}$$

where x_w is the distance measured from the wall.

The air temperature and the water vapor mass fraction at the inlet of the channel are specified to be the ambient, atmospheric temperature, and mass fraction (i.e., calculated from knowledge of the relative humidity), and the air temperature and mass fraction gradients are set to vanish at the exit of the channel.

Heat and mass-transfer parameters

The local heat exchange between the air stream and the water film depends on two related factors: the interfacial temperature gradient on the air side results in sensible convective heat transfer, and the evaporative mass transfer rate on the water film side results in latent heat transfer. The total (sensible and latent) convective heat transfer rate from the film interface to the air stream can be expressed as follows:

$$q(y) = q_s(y) + q_l(y) = -k\frac{\partial T}{\partial x} - \left[\frac{\rho D}{(1-\omega_i)}\frac{\partial \omega}{\partial x}\right]h_{fg} \qquad \text{at} \qquad x = 0 \tag{16}$$

In terms of the local heat h_y and mass g_y transfer coefficients, the local total heat flux at the hot, wet wall can be expressed as follows:

$$q(y) = h_y[T_i(y) - T_b(y)] + \frac{g_y \rho}{(1-\omega_i)}[\omega_i(y) - \omega_b(y)]h_{fg} \tag{17}$$

where the subscript i denotes the quantities at the water film–air interface, and the local bulk temeprature T_b and mass fraction ω_b in the channel are defined as follows:

$$T_b(y) = \int_0^W \rho c_p v T \, dx \Big/ \int_0^W \rho c_p v \, dx \tag{18}$$

and

$$\omega_b(y) = \int_0^W \rho v \omega \, dx \Big/ \int_0^W \rho v \, dx \tag{19}$$

respectively.

If the water film is assumed to be negligibly thin ($\delta \to 0$), the interface temperature T_i will approach that of the hot, wet wall temperature T_w (i.e., $T_i \to T_w$). If the temperature drop across the film is sufficiently large, the interface temperature T_i would have to be predicted by coupling the transport in the film to that in the air stream (Yan et al. 1989; Tsay and Lin 1990; Yan 1995b). For the purpose of generalizing the heat transfer results, the local Nussel number along the wetted wall is defined as

$$\mathrm{Nu}_y = \frac{h_y D_h}{k} = \frac{2Wq_s}{k[T_w(y) - T_b(y)]} \tag{20}$$

Basing the local mass-transfer coefficient on the diffusive mass flux, the local Sherwood number is expressed as

$$\mathrm{Sh}_y = \frac{g_y D_h}{D} = -\frac{2W}{[\omega_w(y) - \omega_b(y)]}\frac{\partial \omega}{\partial x} = \frac{2Wm_w(1-\omega_w)}{D\rho[\omega_w(y) - \omega_b(y)]} \tag{21}$$

Method solution

A control volume, finite-difference numerical integration technique is used to solve the model equations with appropriate boundary conditions. The SIMPLER algorithm is employed to solve the model equations in primitive or dimensional variables; this is discussed in detail by Patankar (1980). The method of solution is detailed elsewhere (Mohamad and Viskanta 1992) and needs not be repeated here. Suffice it to mention that in order to improve the resolution of dependent variables in the turbulent boundary layers, a nonuniform grid is employed. Grid independence of the results is established by employing different size meshes, ranging from 51×101 to 101×401.

It is necessary to mention that the SIMPLER method adopted for the numerical solution of the transport equations is not extremely robust for low-Reynolds number or mixed-convection flows, and the intimate coupling of model equations causes additional difficulties. In addition, the k-ε turbulence model equations are highly nonlinear and must be solved simultaneously with the transport equations. This required a large number of iterations to obtain converged solutions.

Results and discussion

Comparison of model predictions with experimental data

Recently, experimental heat and mass-transfer data have been reported by Ambrosini et al. (1995) for turbulent forced convection in an asymmetrically heated, vertical parallel-plate channel. This provides an opportunity to compare the model predictions against the published experimental average heat and mass transfer data. The channel had a cross section of 60 × 10 cm and was 200-cm high. Experiments were performed with one channel wall fully wetted, and the opposite wall was adiabatic. Air velocities tested were up to 10 m/s. Average Nusselt and Sherwood numbers over the 2-m height of the channel were reported. Local velocity, temperature, mass fraction, and transport quantities were not reported by Ambrosini et al.; therefore, comparisons of the present two-dimensional (2-D) model predictions with the experimental data can be given only for the average Nusselt and Sherwood numbers.

Comparisons of the numerically predicted Nusselt and Sherwood numbers with the results calculated from the corresponding correlations are given in Figures 2 and 3, respectively. Numerically predicted results are reported for two different ways of calculating the average transport quantities: 1) averaging of the local transport coefficients over the height of the channel; and 2) using the logarithmic mean driving potential difference along the length of the channel to define the average coefficient. For example, in the case of the heat transfer, the average convective coefficient is calculated from

$$\bar{h} = \int_0^H h_y (T_w - T_b)\,dy \Big/ \int_0^H (T_w - T_b)\,dy \tag{22}$$

where T_w is the imposed wall temperature. In the Ambrosini et al. (1995) tests and in the present calculations, T_w was held constant, but the bulk temperature T_b and mass fraction ω_b increased with the distance along the channel (see definitions of T_b and ω_b given by Equations 18 and 19. Note that Equation 22 does not reduce to a simple arithmetic average convective coefficient over the height of the channel. To account for the variation of the wall and bulk fluid temperatures along a channel in calculating the heat transfer rate and the average convective coefficient the logarithmic mean temperature difference is often employed in the literature (Kreigh and Bohn 1986). The heat

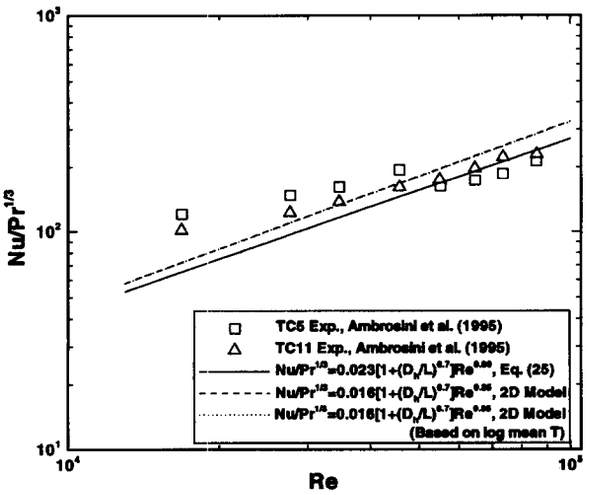

Figure 2 Comparison of average Nusselt number predictions with experimental data

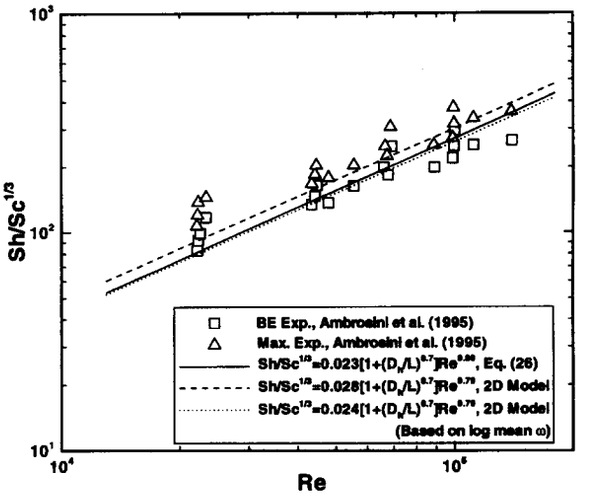

Figure 3 Comparison of average Sherwood number of experimental data

transfer rate from the channel wall to the fluid can be expressed as follows:

$$Q = \tilde{h} A \,\mathrm{LMTD} \tag{23}$$

where $\tilde{h}$ is the simple arithmetic average heat transfer coefficient

$$\left(\tilde{h} = \int_0^H h_y\,dy/H\right)$$

and A is the surface area. The logarithmic mean temperature difference (LMTD) is defined as

$$\mathrm{LMTD} = (\Delta T_{\mathrm{out}} - \Delta T_{\mathrm{in}}/\ln(\Delta T_{\mathrm{out}}/\Delta T_{\mathrm{in}}) \tag{24}$$

where ΔT_{out} and ΔT_{in} are the temperature differences between the wall and bulk temperature of the coolant at the channel outlet and inlet, respectively. For the sake of consistency, the logarithmic mean mass fraction difference was also used to evaluate the average mass transfer coefficient and the average Sherwood number for the channel.

The model predictions and the experimental data of Ambrosini et al. (1995) are compared with the results of the semi-empirical theory for short ducts (Kreith and Bohn 1986), which gives the following expressions for the average Nusselt and Sherwood numbers.

$$\mathrm{Nu}/\mathrm{Pr}^{1/3} = 0.023[1 + (D_h/H)^{0.7}]\mathrm{Re}^{0.8} \tag{25}$$

and, using heat and mass transfer analogy,

$$\mathrm{Sh}/\mathrm{Sc}^{1/3} = 0.023[1 + (D_h/H)^{0.7}]\mathrm{Re}^{0.8} \tag{26}$$

respectively. In these equations, the Nusselt, Sherwood, and Reynolds numbers are all based on the hydraulic diameter D_h as the characteristic length. It should be mentioned that Ambrosini et al. (1995) employed the well-known film theory correction factor to account for the blowing effect (Bird et al. 1960) when reducing their experimental mass-transfer data. There is less scatter in the heat transfer data (Figure 2) around Equation 25 than of mass-transfer data (Figure 3) around Equation 26. For lower-Reynolds number (Re < 50,000), the convective heat trans-

fer for the dry plate appears to be conservatively underpredicted by the correlation, at some Reynolds numbers by, as much as 20% or higher. For mass transfer both "best estimate" and "experimental max" results (Ambrosini et al. 1995) were included in the comparison of the "short duct theory" correlating Equation 26 with test data. The "best estimate" (BE) data are well represented by the correlation. The experimental maximum and best estimate data appear close to each other, but the maximum data are, in general, about 10–20% higher than the best estimate results. No experimental uncertainties or average and maximum departure estimates of the data from the correlation were included in the paper.

Inspection of Figures 2 and 3 reveals that there is some difference in the Nusselt and Sherwood numbers calculated using the two averaging methods. The difference is somewhat smaller for heat transfer than for mass transfer. In all cases, the dependence of thermophysical properties on temperature and mass fraction is accounted by evaluating the average film temperature and mass fraction along the channel and basing the properties on these values. The results show that there is good agreement between theoretically calculated results and the correlations based on the theory for short ducts. The average Sherwood numbers based on the logarithmic mean mass fraction difference are somewhat smaller than those based on the averaging of local mass-transfer coefficients along the channel height, but the reason for the difference is not known. The average Nusselt and Sherwood numbers calculated by the present 2-D model are well represented by Equations 25 and 26, respectively. The k-ε turbulence model can simulate average transport coefficients under turbulent forced-convection conditions with the experimental uncertainty of the data. However, there seem to be some systematic trends that must be explained. For this reason, local heat and mass-transfer results are presented and sensitivity calculations are reported and discussed.

Local transport

Local development of the velocity, temperature, and mass fraction profiles from initially uniform values ($v_o = 4\ m/s$, Re = 41,400) provides no new physical insights beyond those already existing in the literature (Cebeci and Bradshaw 1984) and therefore, are, not included. A fully developed velocity distribution is not expected and was not obtained at the exit of the channel ($y = 2.0$ m). This is due in part to the mass addition to the stream at the wetted wall where water evaporates. The velocity profile is nearly symmetric about the centerline ($y = 0.05$ m) of the channel, because the rate of water evaporation is relatively small compared to the air-flow rate. The velocity distributions reveal steep gradients near the walls and an increase in boundary-layer thickness with the distance along the channel. For the imposed conditions, buoyancy has a little effect on velocity distributions in the channel, and the flow can be considered as being forced. The temperature and water vapor mass fraction profiles develop along the channel, but at the exit (i.e., at a distance of $y/D_h \simeq 12.7$) the effect of the heated wet (left) wall has not yet penetrated to the midplane of the channel, and the profiles continue to develop. The right wall of the channel is adiabatic (also impermeable) and remains at the inlet air temperature.

The sensible, latent, and total heat flux distribution at the heated, wet wall are illustrated in Figure 4. The graphic results of Figure 4 show that the fluxes decrease rapidly with the distance along the channel, because of the growth of the temperature and concentration boundary layers. The transition from laminar to turbulent flow occurs at about $y/H = 0.08$ from the channel entrance. As the flow transitions from laminar to turbulent, the fluxes increase rapidly and reach a secondary maximum at about

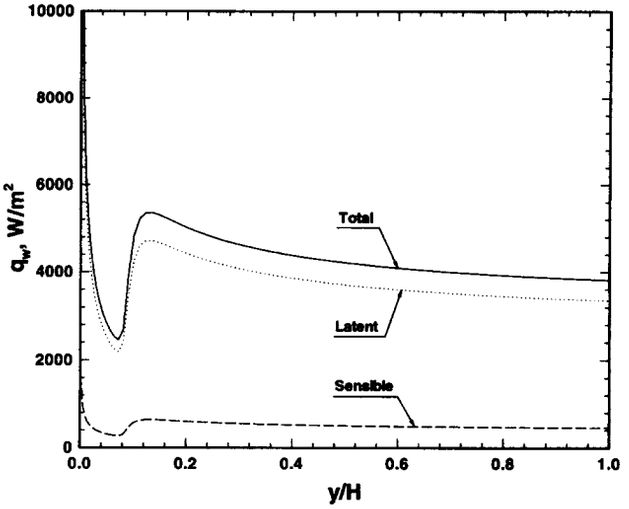

Figure 4 Variation of local sensible, latent, and total heat fluxes along the channel for $v_o = 4.0$ m/s, $T_w = 50°C$, $T_o = 20°C$, $\phi_o = 50\%$, and $H/W = 20$ ($H = 2.0$ m and $W = 0.1$ m)

$y/H = 0.14$ m and decrease very gradually from this point on. Under the imposed conditions considered, sensible heat flux accounts for only about 10% of the total heat flux.

The effect of the channel inlet velocity v_o (i.e., Reynolds number) on the local Nusselt number is illustrated in Figure 5. As the Reynolds number increases from 10,300 to 82,900 the transition point from laminar to turbulent flow moves upstream from about $y/H = 0.56$ to $y/H = 0.01$, respectively. The local Nusselt number distributions along the channel, of course, affect the average values shown in Figure 2, which are represented by empirical equations obtained by a least-squares fit of the average, numerically calculated Nusselt numbers.

A comparison of local Nusselt and Sherwood numbers along the hot, wetted channel wall is given in Figure 6 ($v_o = 4$ m/s, Re = 41,400). In the turbulent flow regime ($y/H > 0.12$) and the conditions considered, the local Sherwood number is on average about 10% smaller than the Nusselt number. Furthermore, the difference increases with the distance along the channel. This is more clearly illustrated in Figure 7 where the Sh_y/Nu_y ratio

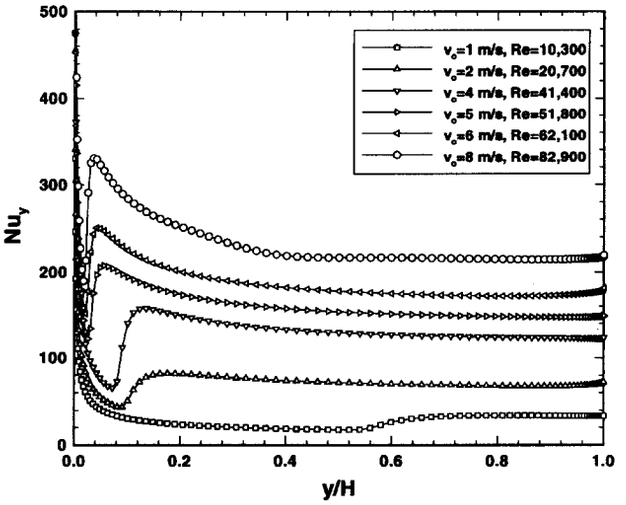

Figure 5 Effect of channel inlet velocity v_o (Reynolds number) on the local Nusselt number for $T_w = 50°C$, $T_o = 20°C$, $\phi_o = 50\%$, and $H/W = 20$ ($H = 2.0$ m and $W = 0.1$ m)

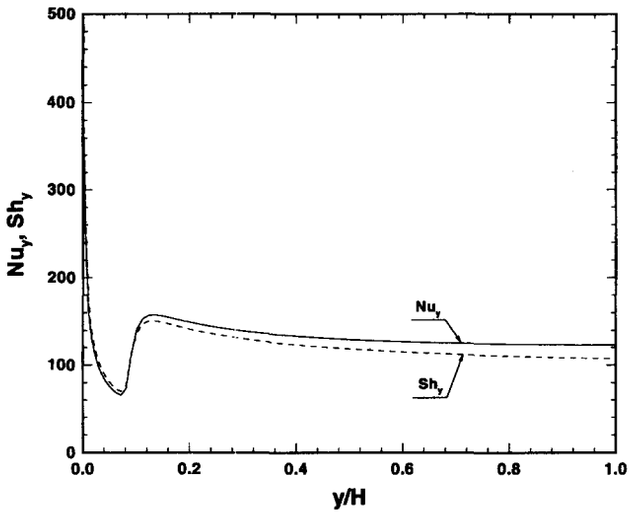

Figure 6 Comparison of local Nusselt and Sherwood numbers for $v_o = 4.0$ m/s (Re = 41,400) $T_w = 50°C$, $T_o = 20°C$, $\phi_o = 50\%$, and $H/W = 2.0$ ($H = 20$ m and $W = 0.1$ m)

along the channel is presented for several Reynolds numbers. The trends in the Sh_y/Nu_y ratio suggest that the results do not follow the heat and mass-transfer analogy for small mass-transfer rates, which predicts that $Sh_y/Nu_y = (Sc/Pr)^{1/3}$ (see Equations 25 and 26). For the imposed conditions and results shown in Figure 7, $Pr = 0.702$ and $Sc = 0.559$. Hence, $Sh_y/Nu_y = (0.559/0.702)^{1/3} = 0.927$. The reasons for the difference between the predictions and the heat and mass-transfer analogy revealed in the figure are not known, but the dependence of Sh_y/Nu_y on the distance along the channel cannot be accounted for by the variation of the thermophysical properties with temperature and water vapor concentration.

Effect of buoyancy

The results of Figures 2 and 3 reveal that at lower-Reynolds numbers (Re < 30,000), the model underpredicts the average transport coefficients. This may be attributable to the action of the buoyancy force in the vicinity of the hot, wet wall, which distorts the flow and, simultaneously, the thermal and solutal fields. To check on this effect, the buoyancy force was included in the y-momentum Equation 3. As a sample calculation, the predicted development of the velocity profile for mixed convection is illustrated in Figure 8 ($v_o = 2$ m/s, Re = 10,300). The results show that the velocity profile is not symmetrical about the midplane ($x/W = 0.5$) of the channel but is skewed. The velocity is higher near the heated, wet wall than near the adiabatic wall. The dimensionless temeprature and mass fraction profiles along the channel are also affected by the velocity profile modified by the presence of the buoyancy force, but this cannot be clearly revealed by the profiles. Instead, the local Nusselt and Sherwood number for forced (without buoyancy) and mixed (with buoyancy) convection are compared in Figure 9. Numerical results presented in Figure 9 reveal several interesting features that the buoyancy force introduces to the flow. Accounting for buoyancy in the mixed convection simulation leads to an increase in the local Nusselt and Sherwood numbers in the laminar flow regime ($y/h \lesssim 0.4$) compared to those for the pure forced-convection simulation (buoyancy term is disregarded in Equation 3). However, the presence of the buoyancy force delays the transition from laminar to turbulent flow and also decreases the local Nusselt and Sherwood numbers for $y/H \gtrsim 0.7$ (i.e., turbulent flow regime). This suggests that the buoyancy force plays a stabilizing role by delaying the transition from laminar to turbulent flow.

Effect of inlet turbulence

For the results presented, the turbulence intensity at the inlet was assumed to vanish ($Tu_o = 0\%$); however, in the experiments, there were made no special precautions to eliminate the turbulence at the inlet to the channel, and the intensity is expected to be finite. To examine the effect of Tu_o, calculations have also been performed for Tu_o equal to 0 and 1%, and the results are given in Figure 10. The results show that the presence of turbulence at the inlet to the channel causes flow transition to occur closer to the channel inlet. For example, at $Tu_o = 0\%$ the flow transitions from laminar to turbulent at $y/H \simeq 0.56$; whereas, for $Tu_o = 1\%$ the transition occurs at $y/H \simeq 0.18$. As a conse-

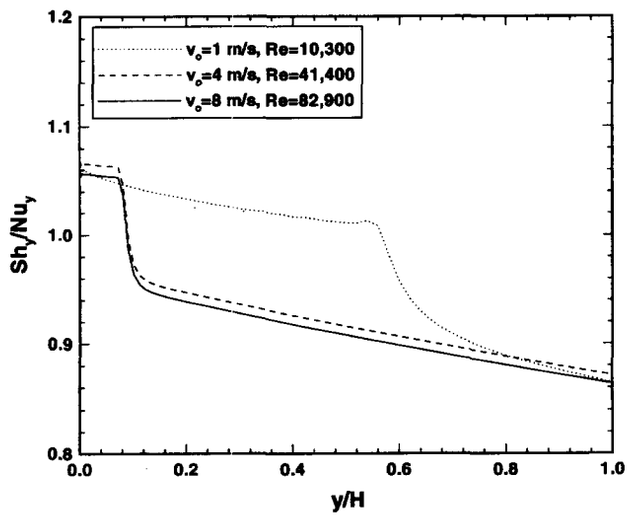

Figure 7 Effect of inlet velcoity v_o (Reynolds number) on the local Sherwood-to-Nusselt number ratio for $T_w = 50°C$, $T_o = 20°C$, $\phi_o = 50\%$, and $H/W = 20$ ($H = 2.0$ m and $W = 0.1$ m)

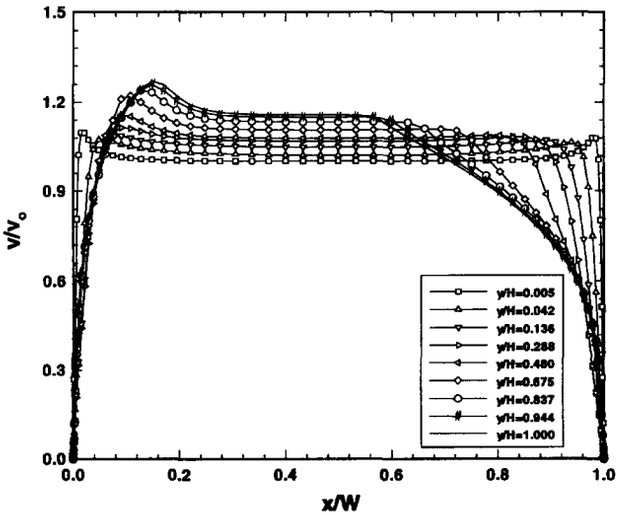

Figure 8 Vertical velocity distributions along the channel for mixed convection for $v_o = 1.0$ m/s (Re = 41,400) for $T_w = 50°C$, $T_o = 20°C$, $\phi_o = 50\%$, and $H/W = 20$ ($H = 2.0$ m and $W = 0.1$ m)

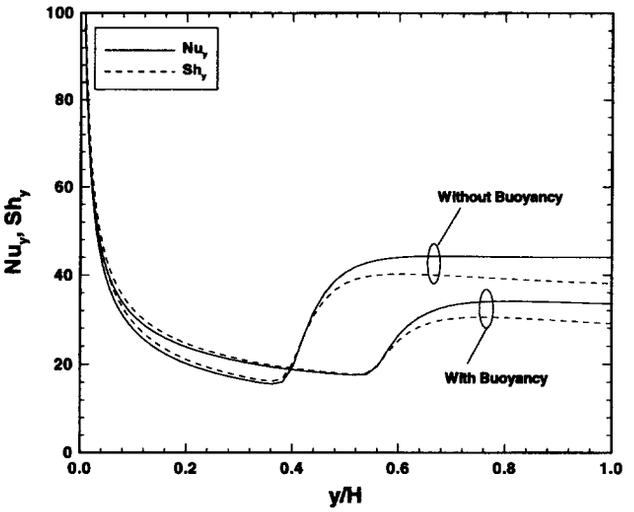

Figure 9 Variation of local Nusselt and Sherwood numbers for forced (without buoyancy) and mixed (with buoyancy) convection (see Figure 8 for conditions)

quence, the average Nusselt and Sherwood numbers would be increased by the presence of turbulence at the inlet to the channel. This is consistent with the average Nu and Sh numbers presented in Figures 2 and 3, respectively. The results of calculations show that the turbulence at the channel inlet increases the transport coefficients.

The average Nusselt number for $Tu_o = 0\%$ and $Tu_o = 1\%$ are 30.82 and 37.36, respectively; whereas, the average Sherwood numbers for $Tu_o = 0\%$ and $Tu_o = 1\%$ are 28.91 and 34.38, respectively. Thus, the increase in the average transport parameters by the turbulence at the inlet to the channel seems to be consistent with the average experimental values presented in Figures 2 and 3. Unfortunately, the turbulent intensity at the channel inlet was not measured by Ambrosini et al. (1995) in their experiments. Therefore, a quantiative comparison of the effect of inlet turbulence on the average Nusselt and Sherwood numbers cannot be assessed.

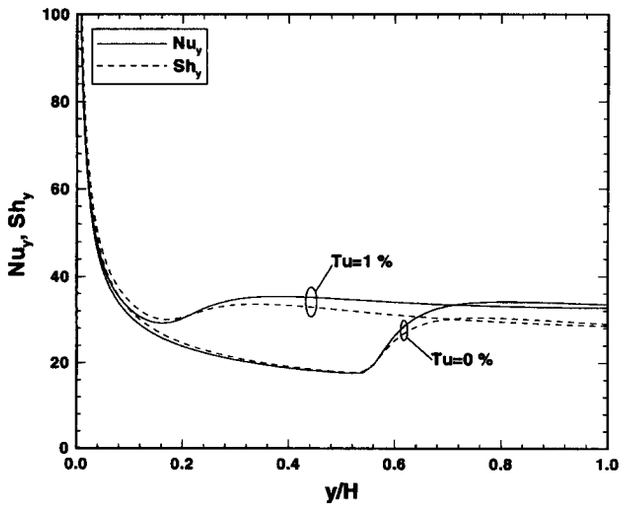

Figure 10 Effect of inlet turbulence on local Nusselt and Sherwood number variation along the channel (see Figure 8 for conditions)

Conclusions

Turbulent convection heat and mass-transfer characteristics in an asymmetrically heated, wet, vertical, parallel-plate channel have been studied. Based on the numerical results obtained, the following conclusions can be drawn.

(1) Heat transfer from the liquid film is dominated by the transport of latent heat associated with the evaporation of the liquid film.
(2) The results obtained suggest that the heat and mass transfer analogy begins to break down after the flow transitions from laminar to turbulent.
(3) Initial turbulence in the air stream moves the critical point for transition from laminar to turbulent flow closer to the inlet and affects the average transport coefficients.
(4) At lower Reynolds numbers (Re < 30,000) the buoyancy aids the flow, distorts (skews) the velocity distribution and affects transport coefficients.
(5) Detailed experimental flow, heat, and mass-transfer data are needed to validate 2-D transport analysis and the appropriateness of the low Reynolds number k-ε turbulence model. The greatest computational uncertainty is in the prediction of the correct location for transition from laminar to turbulent flow.

Acknowledgments

This work was supported in part by the U.S. Nuclear Regulatory Commission through a contract to Energy Research, Inc. The authors acknowledge helpful discussions with M. Khatib-Rahbar, A. Notafrancesco, and J. Tills.

References

Ambrosini, W., Manfredini, A., Mariotti, F. and Oriolo, F. 1995. Heat transfer from a plate cooled by a water film with countercurrent air flow. *Nuclear Technol.* **112**, 227–237

Bird, R. B., Stewart, W. E. and Lightfoot, E. N. 1960. *Transport Phenomena*. John Wiley, New York, 658–668

Cebeci, T. and Bradshaw, P. 1984. *Physical and Computational Aspects of Convective Heat Transfer*. Springer-Verlag, New York, 592

Eckert, E. R. G. and Drake, R. M. 1972. *Analysis of Heat and Mass Transfer*. McGraw-Hill, New York, 806

Jones, W. P. and Launder, B. E. 1973. The calculation of low-Reynolds number phenomena with a two-equation model of turbulence. *Int. J. Heat Mass Transfer*, **16**, 1119–1130

Kreith, F. and Bohn, M. S. 1986. *Principles of Heat Transfer*, 4th ed. International Textbook, Scranton, PA, 323–327

Launder, B. E. 1988. On the computation of convective heat transfer in complex turbulent flows. *J. Heat Transfer*, **110**, 1112–1128

Mohamad, A. A. and Viskanta, R. 1992. Application of low Reynolds number k-ε turbulence model to buoyant and fixed flows in a shallow cavity. In *Fundamentals of Mixed Convection*, T. S. Chen and T. Y. Chen (eds.), HTD, Vol. **213**, ASME, New York, 43–54

Patankar, S. V. 1980. *Numerical Heat Transfer and Fluid Flow*. Hemisphere, Bristol, PA

Patel, V. C., Rodi, W. and Schenerer, G. 1985. Turbulence models for near-wall and low-Reynolds number flow: A review. *AIAA J.* **23**, 1308–1319

To, W. M. and Humphrey, J. A. C. 1987. Numerical simulation of buoyant, turbulent flow—I. Free convection along a heated vertical plate. *Int. J. Heat Mass Transfer*, **25**, 221–231

Tsay, Y. L. and Lin, T. F. 1990. Combined heat and mass transfer in laminar gas stream flowing over an evaporating liquid film. Wärme-und Stoffübertragung, **25**, 221–231

Yan, W. M., Tsay, Y. L. and Lin, T. F. 1989. Simultaneous heat and mass transfer in laminar mixed convection flows between vertical parallel plates with asymmetric hating. *Int. J. Heat Fluid Flow*, **10**, 262–269

Yan, W. M. 1991. Mixed convection heat and mass transfer in a wetted channel, *Canadian J. Chem. Eng.*, **69**, 1277–1282

Yan, W. M. 1995a. Turbulent mixed convection heat and mass transfer in a wetted channel. *J. Heat Transfer*, **117**, 229–233

Yan. W. M. 1995b. Effect of film vaporization on turbulent mixed convection heat and mass transfer in a vertical channel. *Int. J. Heat Mass Transfer*, **38**, 713–722